ACS OMEGA

Open Access

http://pubs.acs.org/journal/acsodf

Article

Effect of High Calcium and High Iron Coal on Ash Fusion Characteristics of Petroleum Coke during Cogasification

Bing Wang,* Cuiyu Zhao, and Congxiu Guo

Cite This: *ACS Omega* 2024, 9, 33090−33098

Read Online

ACCESS | Metrics & More | Article Recommendations

ABSTRACT: Entrained flow gasification provides a more efficient utilization method for high-sulfur petroleum coke. The operation temperature of the entrained flow gasifier must be above the ash fusion temperature (AFT) of petroleum coke due to the liquid slag discharge. In this work, petroleum coke was blended with high-calcium coal and high-iron coal, respectively, under a reducing atmosphere, and the variations in AFTs were recorded by an ash fusion temperature analyzer. The influence of mineral transformations on the ash fusion characteristics of blended ash was analyzed by X-ray diffraction and FactSage. The results showed that both high calcium coal and high iron coal could efficiently reduce the AFTs of petroleum coke. When the ratio of high calcium coal and high iron coal reached 60 wt %, the corresponding flow temperature (FT) of mixed ash decreased to 1225 and 1312 °C, respectively. With the content of high calcium coal increasing, coulsonite (FeV_2O_4), vanadium trioxide (V_2O_3) and nickel (Ni) with high-melting points tended to decrease, causing the decrease of AFT for mixed ash. As high iron coal was added, Ni and V_2O_3 continuously kept decreasing. In particular, the percentage of FeV_2O_4 first increased and thereafter decreased with high iron coal above 40 wt %.

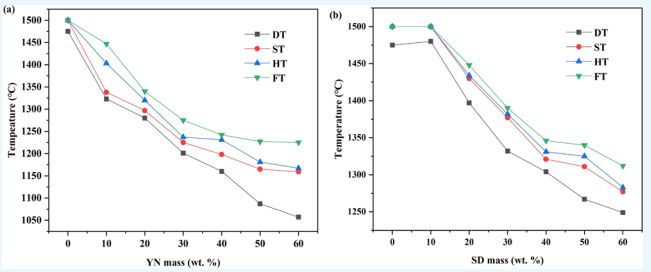

1. INTRODUCTION

With the modern industry developing, energy consumption is increasing rapidly.[1,2] Oil, as a typical fossil energy, possesses a high level of consumption. The quality of crude oil is deteriorating gradually due to its increasing consumption yearly. Petroleum coke, one of the byproducts of petroleum refining, is directly used for industry fuel.[3] The yield of the petroleum coke grows heavily since oil refineries continuously process heavy oil. However, high-sulfur petroleum coke, which accounts for more than 60% of China's production, will inevitably release large amounts of sulfur oxides and nitrogen oxides into the environment when combusted directly.[2] Thus, it is important to develop an efficient and environmentally friendly way to utilize petroleum coke.

Petroleum coke, which possesses high carbon content, high heat value, and low ash content, can be converted into syngas through gasification technology.[4] Besides, high-sulfur petroleum coke will produce elemental sulfur to reduce pollutant emissions when gasified.[5] Due to the low gasification activity of petroleum coke, entrained flow gasifiers with high carbon conversion efficiency and thermal efficiency are essential for the gasification reaction of petroleum coke.[6,7] The operational stability of the entrained flow gasifiers is greatly affected by the ash fusion characteristics of petroleum coke.[8] Continuous liquid slag discharge is imperative so that the ash slagging temperature of petroleum coke must be lower than the operation temperature of entrained flow gasifiers.[9] Petroleum coke ash mainly includes Si, Al, Ni, V, and Ca. Specially, the content of V in the petroleum coke ash is generally more than 20 wt %, which leads to a different transformation behavior of V from the usual ash at high temperatures and may cause unpredictable ash-related problems such as slagging, fouling, bed agglomeration, and so on during the gasification process.[10] Frandsen et al. found that V_2O_3 was the main species below 1477 °C at the reduced atmosphere according to the thermal conversion calculations.[11] Li et al. studied the transformation behavior of V during the gasification based on the experiments and thermodynamic calculations[12] and concluded that V_2O_3 as the formed V-bearing mineral was mainly present. In addition, the influence of V on the ash fusion characteristics under reduced conditions has also attracted much attention. Li et al. and Wang et al. found that as the content of V_2O_5 increased, the ash fusion temperature (AFT) prominently increased.[4,13] When the content of V_2O_5 was 25 wt %, the flow temperature was over 1450 °C. The role that V_2O_5 plays in ash fusion process has been much studied, but there is little research on the ash fusion characteristics of petroleum coke.

Received: May 10, 2024
Revised: July 1, 2024
Accepted: July 3, 2024
Published: July 17, 2024

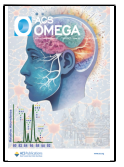

Table 1. Proximate and Ultimate Analysis for Raw Materials

	Proximate analysis (wt %)			Ultimate analysis (wt %)				
Samples	Moisture	Ash	Volatile matter	C	H	O	N	S
DQ	0.13	0.21	7.74	91.43	4.27	1.34	1.58	0.373
YN	12.63	14.88	43.67	51.46	4.87	19.82	1.65	2.25
SD	2.12	10.69	41.22	80.85	5.34	10.732	1.08	1.98

Table 2. Compositions for the Prepared Ash Samples (wt %)

Sample	V_2O_5	NiO	SiO_2	Al_2O_3	Fe_2O_3	CaO	MgO	TiO_2	SO_3	K_2O	Na_2O	P_2O_5
DQ	32.35	9.75	17.74	7.04	5.35	21.35	0.74	0.74	0.97	1.35	1.05	0.61
YN	0.27	0.12	33.12	24.25	6.73	21.64	4.26	0.76	3.43	1.03	3.79	0.21
SD	0.12	0.07	38.46	26.34	22.49	5.45	1.13	0.38	1.23	1.37	2.25	0.39

Petroleum coke with a high V content usually has a high AFT, which affects its industrial application in the entrained flow gasifiers. Recently, the cogasification of petroleum coke with coal has been applied to improve the ash fusion characteristics of petroleum coke.[14−16] It has been reported that coal can reduce the AFT and improve the reactivity of petroleum coke to meet the demand for liquid slagging.[16] Li et al. blended petroleum coke with three Chinese coals to investigate the effects of coal ash, coal ratio, coal rank, and coal char types on cogasification reactivities.[17] The synergistic interactions, which existed in the cogasification process of coal and petroleum coke, significantly improved the gasification reactivity of petroleum coke and were related to the alkali index of coal ash. A similar result was also demonstrated by Kang et al.[18] Apart from the influence of coal on increasing the reactivity, slagging blockage and refractory erosion can also be alleviated since coal has effects on the crystallization and viscosity of slag by adjusting the mineral transformation behaviors of petroleum coke during the cogasification process.[19,20]

Based on the large surface area and high content of alkali metal, coal has effects on the gasification reactivity and ash fusion characteristics of petroleum coke. Herein, the impact of coal on the ash fusion characteristics of petroleum coke was studied by blending the petroleum coke ash with high calcium coal ash and high iron coal ash, respectively, under a reducing atmosphere. The relationship between mineral transformations and ash fusion characteristics was analyzed by X-ray diffraction. In addition, FactSage thermodynamic equilibrium calculations were used to simulate the ash fusion process. These may elucidate the experimental results.

2. EXPERIMENTS AND CHARACTERIZATIONS

2.1. Preparation of Ash Samples. Petroleum coke from Daqing Oilfield, China, high-calcium coal from Xiaolongtan, Yunnan Province, China, and high-iron coal from Yanzhou, Shandong Province, China, were used in this work and designated as DQ, YN, and SD, respectively. The corresponding proximate and ultimate analyses on an air-dried basis are shown in Table 1. Petroleum coke ash was determined according to the American Society of the International Association for Testing and Materials (ASTM-International) standard designation D4422−13, Standard Test Method for Ash in Analysis of Petroleum Coke. The high calcium and high iron coal ashes were obtained based on the Chinese standard procedures (GB/T 1574−2007). The compositions of three sample ashes are summarized in Table 2. To investigate the effect of coal on the AFT behavior of petroleum coke, YN and SD ashes were blended with DQ ash with mass ratios ranging from 10 wt % to 60 wt % at the interval of 10 wt %, respectively. After sufficiently blended, the obtained mixture was dried at 105 °C for 24 h under a N_2 atmosphere.

Table 3. AFTs for the Prepared Ash Samples (°C)

Samples	DT	ST	HT	FT
DQ	1475	>1500	>1500	>1500
YN	1173	1186	1191	1230
SD	1200	1232	1277	1305

2.2. Measurements of AFTs. The AFTs of the mixed ashes were determined by the ash fusion temperature analyzer (KY Corporation, China) at reduced atmosphere according to Chinese standard procedures (GB/T 219−2008). During the experimental process, the ash cones with a specific geometry were heated to 900 °C with a heating rate of 15 °C/min and thereafter heated at 5 °C/min without exceeding 1500 °C. Four characteristic temperatures of the ashes including deformation temperature (DT), softening temperature (ST), hemispherical temperature (HT), and flow temperature (FT) were obtained. AFT tests were repeatedly carried out to reduce errors. The error range is within 10 °C.

2.3. Quenching Experiments. The high-temperature ash slag samples were obtained by quenching experiments as the temperatures ranged from 1000 to 1300 °C with a 100 °C interval. The corundum crucible filled with 1.0 g of ash sample was heated by the electric tube furnace at a reducing atmosphere (CO/CO_2 = 6:4). The thermal profiles were set on the basis of the AFT tests. When the set temperature was reached and held for 15 min, the ash slag was instantly removed and quenched by iced water for avoiding phase transformation and crystal segregation.

2.4. Characterizations. The X-ray fluorescence spectrometry (Rh target X-ray tube, 50 kV, 40 mA) from Shimadzu, Japan, could be applied to characterize the chemical compositions of ash samples. The compositions of quenched ashes were tested by powder X-ray diffraction (RIGAKU D/max-rB, Cu Kα radiation, 40 kW, 100 mA) with the step size of 0.01° at a speed of 4° 2θ/min in the 2θ range of 10−80°.

2.5. Thermodynamic Equilibrium Calculations. The proportion variations in solid and liquid phase, multiphase equilibrium, and phase composition for multicomponents were calculated by FactSage. For the equilibrium calculations, 1.0 g of the blended ash sample was used as input data rather than the original mineral compositions in petroleum coke ash and coal ash from our experimental data, assuming that all of the metal elements used could be allowed to freely enter into equilibrium.

https://doi.org/10.1021/acsomega.4c04453
ACS Omega 2024, 9, 33090−33098

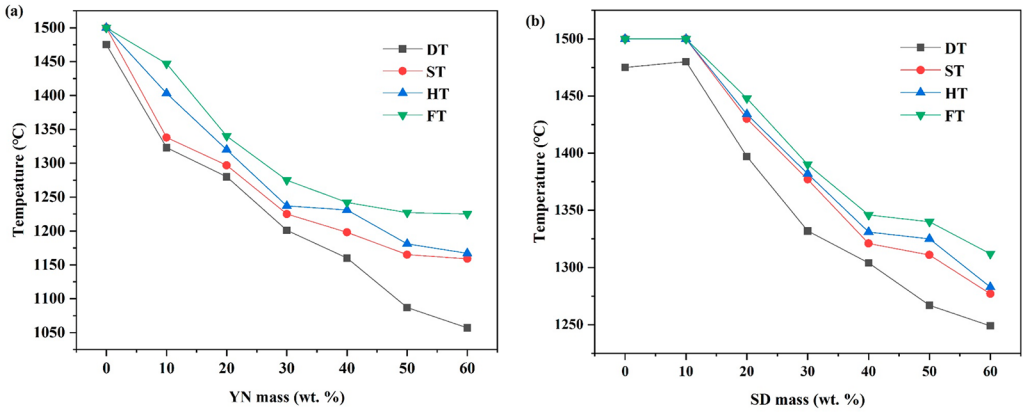

Figure 1. AFT variations of blending DQ ash with different coal ash: (a) YN; (b) SD.

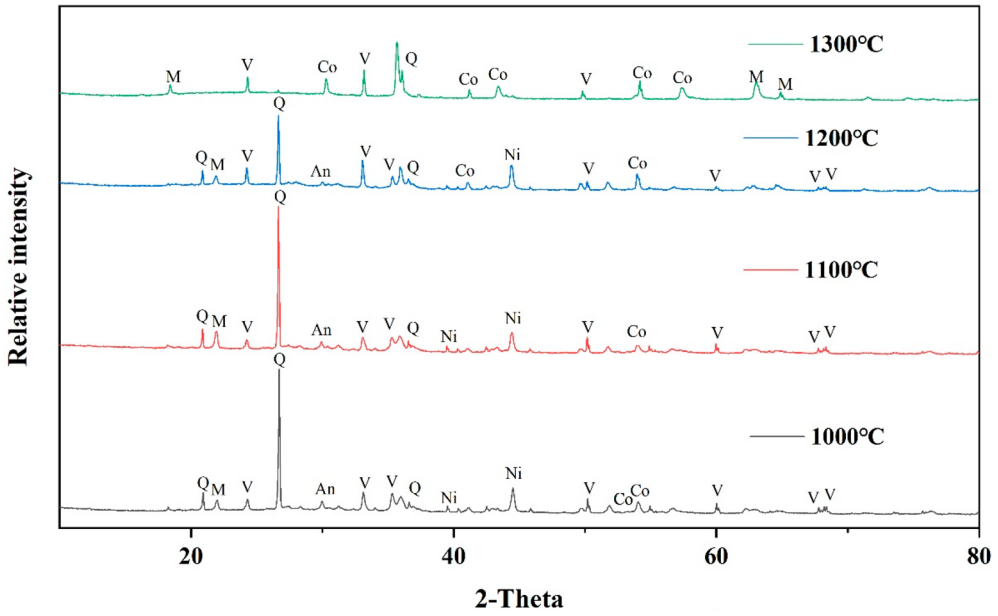

Figure 2. XRD patterns of DQ ash at different temperatures. An: anorthite ($CaAl_2Si_2O_8$); Q: quartz (SiO_2); Co: coulsonite (FeV_2O_4); V: vanadium trioxide (V_2O_3); Ni: nickel (Ni); M: mullite ($3Al_2O_3{\cdot}2SiO_2$).

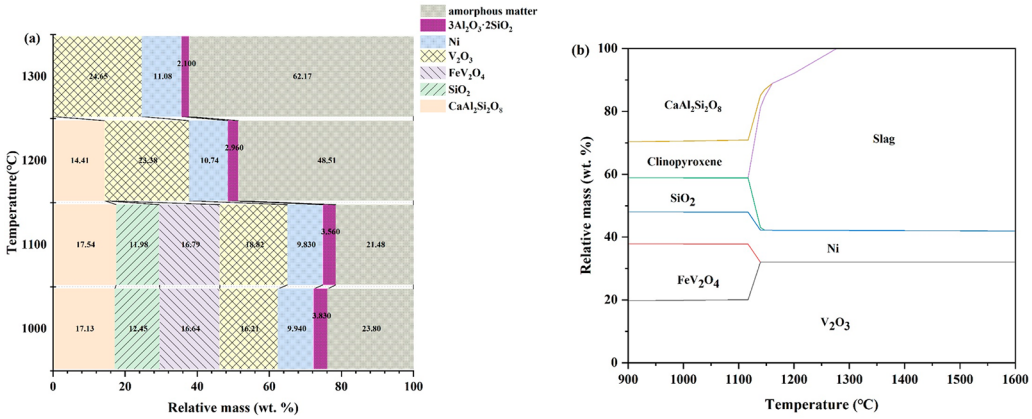

Figure 3. Composition diagram (a) and phase assemblage (b) of DQ ash at different temperatures simulated by FactSage.

For phase formation data, the FToxid and FactPS databases were selected. In lack of the database, the interactions between the VO_x and the slag cannot be analyzed by FactSage. The simulations were performed at reduced atmosphere (CO/CO_2= 6:4) under 0.1 MPa. FactSage operated based on the minimizing Gibbs free energy. Once the total Gibbs energy of the system had reached its minimum, it would be assumed that both homogeneous and heterogeneous chemical reactions reached

https://doi.org/10.1021/acsomega.4c04453
ACS Omega 2024, 9, 33090−33098

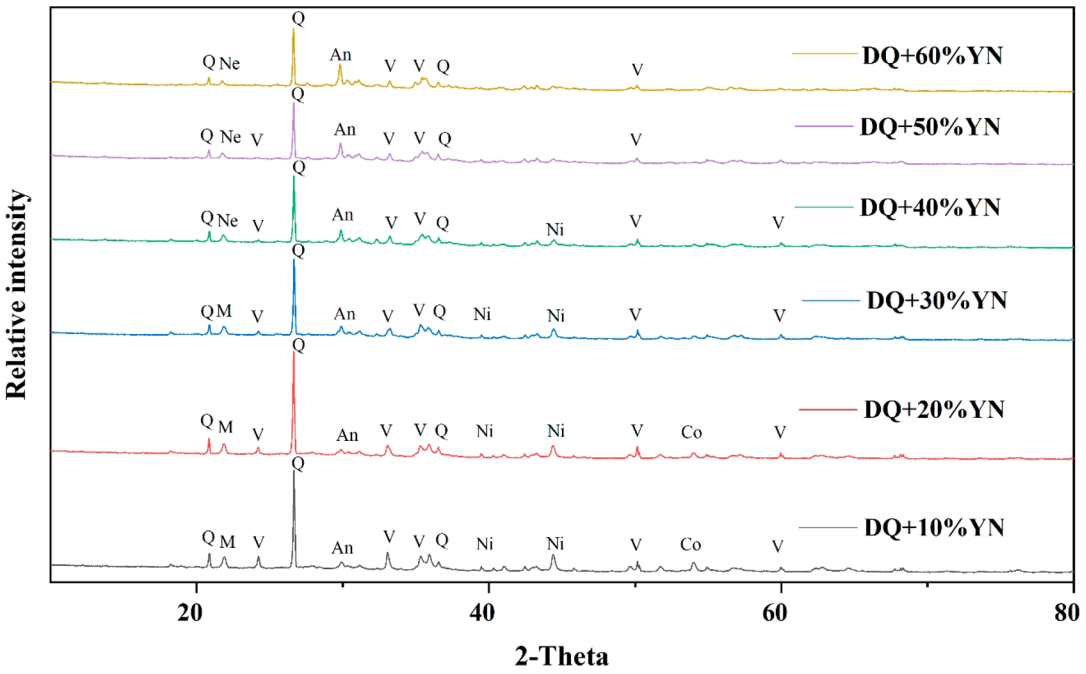

Figure 4. XRD patterns for the mixture of DQ and YN ashes with different ratios at 1100 °C. An: anorthite ($CaAl_2Si_2O_8$); Q: quartz (SiO_2); Co: coulsonite (FeV_2O_4); Ni: nickel (Ni); Ne: nepheline ($NaAlSiO_4$); V: vanadium trioxide (V_2O_3); M: mullite ($3Al_2O_3{\cdot}2SiO_2$).

an equilibrium state in which the chemical species and phases would remain stable.[21] The formed phases were ignored in the calculations if their corresponding equilibrium concentrations were less than 0.01 wt %.

3. RESULTS AND DISCUSSIONS

3.1. AFTs for the Prepared Ash Samples. Table 3 lists the AFTs of ash samples for petroleum coke and coal. The DT of

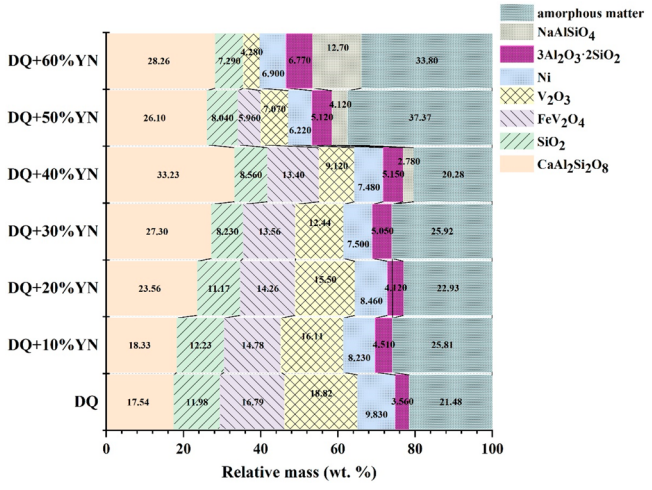

Figure 5. Composition diagram of the mixed ashes with different ratios of YN ashes at 1100 °C simulated by FactSage.

DQ ash reaches 1475 °C, and the ST, HT, and FT are all above 1500 °C, which are higher than the operation temperature of entrained flow gasifiers. In contrast, the AFTs of YN and SD ashes are much lower than those of DQ. Theoretically, the AFTs of petroleum coke could be reduced by coal.

Thus, DQ ash was blended with different mass ratios of YN or SD ash, and the corresponding AFT variations are shown in Figure 1. With the content of YN ash increasing, the AFTs of the mixed ashes decreased continuously. The FT of the blended ash was decreased to 1225 °C at 60 wt % addition of YN ash, which meant that there was an interaction between DQ and YN ashes, and the low-melting minerals may be formed under reducing atmosphere causing the decrease in AFTs of DQ ash. The AFT of the blended ash showed a slight increase when the addition of SD ash was 10 wt %. Conversely, the AFTs decreased steadily with the content of SD ash ranging from 20 to 60 wt %, and the FT was 1312 °C under 60 wt % addition of SD ash. Obviously, the impact of SD ash on the ash fusion characteristics of DQ was similar to that of YN ash.

3.2. Mineral Transformation during the Ash Fusion Process of DQ Ash. The composition and content variations induced by mineral interactions in the mixed ashes at high temperatures can affect the AFTs. It is imperative to study the variations of mineral phases within different temperature ranges during the ash fusion process. Figure 2 displays the mineral composition changes of DQ ash as the reducing temperature ranged from 1000 to 1300 °C. At 1000 °C, coulsonite (FeV_2O_4), anorthite ($CaAl_2Si_2O_8$), nickel (Ni), vanadium trioxide (V_2O_3), and quartz (SiO_2) were the main mineral phases of DQ ashes, among which the content of SiO_2 was the highest. The mineral compositions at 1100 °C were almost the same as those at 1000 °C. When the temperature reached 1200 °C, the diffraction peak of $CaAl_2Si_2O_8$ was weakened, representing a decline. However, FeV_2O_4 and V_2O_3 showed the opposite changes. $CaAl_2Si_2O_8$ disappeared at 1300 °C, and the minerals mainly consisted of V_2O_3, SiO_2 and FeV_2O_4 whose melting points are above 1600, 1500, and 1940 °C, respectively, resulting in high AFTs of DQ ash.[22]

FactSage software was applied to simulate the component distributions and phase assemblages of DQ ash at reduced atmosphere from 1000 to 1300 °C as shown in Figure 3. The ash slag mainly included V_2O_3, SiO_2, $CaAl_2Si_2O_8$, FeV_2O_4, and Ni at 1000 °C according to the simulated calculations in Figure 3a,

https://doi.org/10.1021/acsomega.4c04453
ACS Omega 2024, 9, 33090−33098

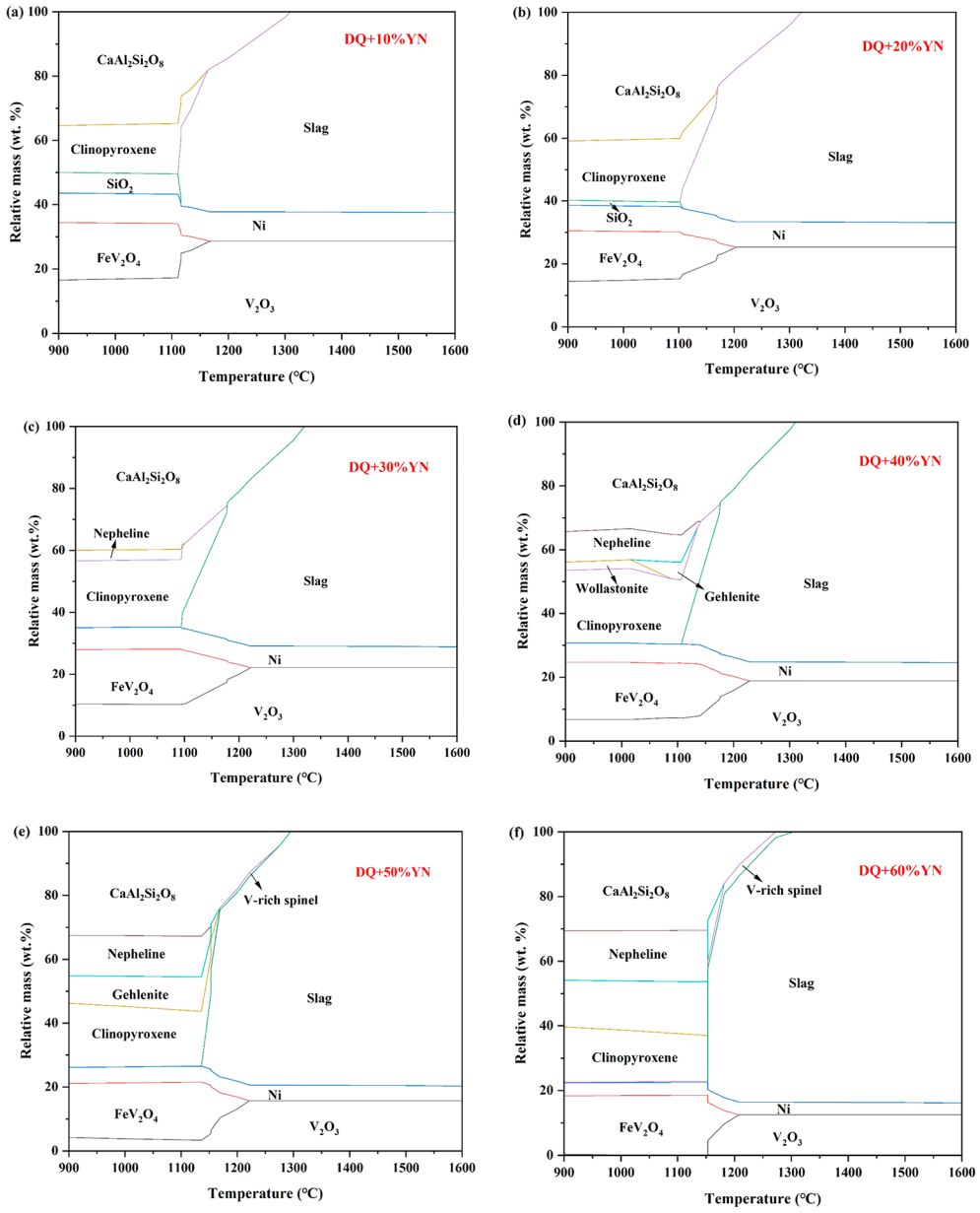

Figure 6. Phase assemblages of the mixed ashes with different ratios of YN ash at different temperatures simulated by FactSage: (a) DQ+10%YN, (b) DQ+20%YN, (c) DQ+30%YN, (d) DQ+40%YN, (e) DQ+50%YN, and (f) DQ+60%YN.

which was consistent with the XRD pattern of DQ ash. With the increase of reducing temperature, the contents of FeV_2O_4, $CaAl_2Si_2O_8$, and SiO_2 gradually decreased. At 1300 °C, FeV_2O_4 and $CaAl_2Si_2O_8$ decomposed and disappeared. Meanwhile, V_2O_3, Ni and mullite ($3Al_2O_3{\cdot}2SiO_2$) were the main minerals. It can be deduced that DQ ash has high AFTs since the ash slag mostly consists of V_2O_3 and Ni with high melting points. The phase assemblages calculated by FactSage software in Figure 3b were almost in accordance with the aforementioned composition distribution simulation. Besides, clinopyroxene formed in the calculated phase assemblages when the reducing temperature was below 1100 °C, and subsequently melted as the temperature increased. FeV_2O_4 decomposed at 1125 °C in the phase assemblage analysis, whereas it was present during the reducing temperature ranges based on the XRD patterns of DQ ash in Figure 2. The difference in the FeV_2O_4 between XRD analysis and FactSage calculation may be due to the fact that the chemical kinetics, temperatures, and composition gradients were not considered by FactSage. In general, the results from FactSage calculations were basically in coincidence with the XRD tests, and high AFTs of DQ ash were influenced by V_2O_3 and Ni.

3.3. Mineral Transformation Behaviors for the Mixture of DQ and YN Ashes. It is expected that the addition of low-melting coal ash may influence the mineral phase composition of the ash slag during the ash fusion process, which afterward improves the ash fusion characteristics of the mixed ash. Figure 4 shows the component variations of the mixture of DQ and YN ashes with different ratios at 1100 °C under a reducing atmosphere. When the content of YN ash was 10 and 20 wt %, the corresponding XRD patterns of the mixed ash showed that the main minerals were still FeV_2O_4, SiO_2, $CaAl_2Si_2O_8$ V_2O_3, and Ni and greatly resembled those of pure DQ ash. With the increase of the YN ash content, the proportion of SiO_2 decreased, which was possibly caused by the fact that low-melting $CaAl_2Si_2O_8$ formed when CaO in YN ash reacted with

https://doi.org/10.1021/acsomega.4c04453
ACS Omega 2024, 9, 33090−33098

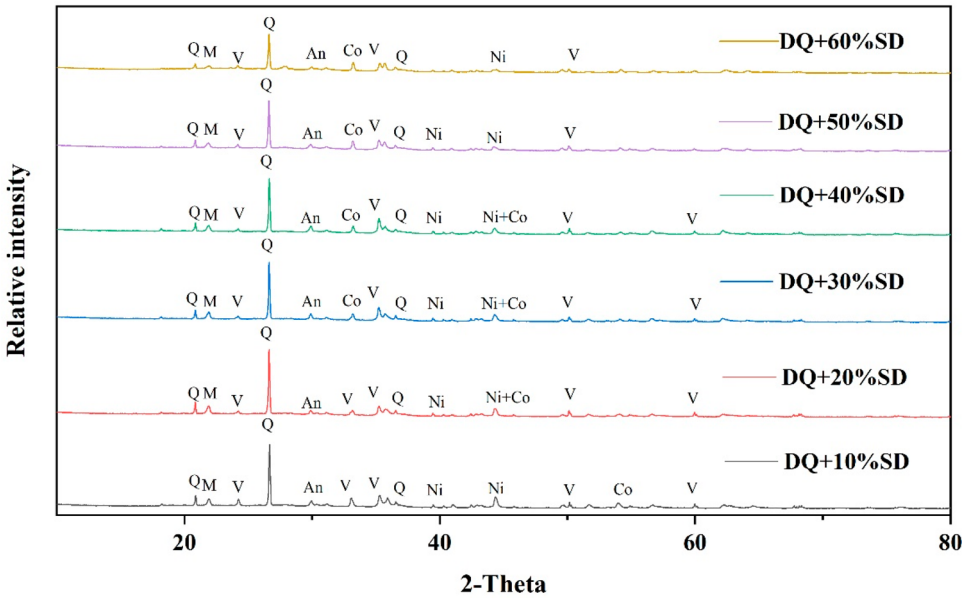

Figure 7. XRD patterns for the mixture of DQ and SD ash with different ratios at 1100 °C. An: anorthite ($CaAl_2Si_2O_8$); Q: quartz (SiO_2); Co: coulsonite (FeV_2O_4); V: vanadium trioxide (V_2O_3); Ni: nickel (Ni); M: mullite ($3Al_2O_3{\cdot}2SiO_2$).

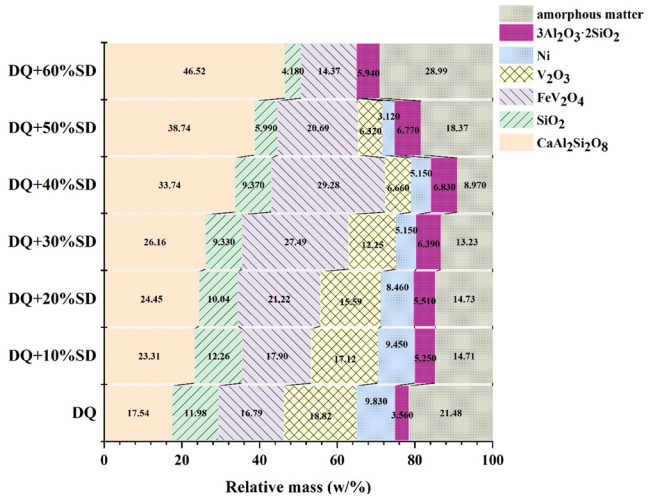

Figure 8. Composition diagram of the blended ashes with different ratios of SD ash at 1100 °C simulated by FactSage.

SiO_2. Besides, the content of $CaAl_2Si_2O_8$ increased and the diffraction peak of high-melting FeV_2O_4 disappeared. The diffraction peaks of nepheline ($NaAlSiO_4$) in ash slag were detected when the addition of YN ash was over 40 wt %. Furthermore, Ni vanished, and the contents of SiO_2 and V_2O_3 decreased continuously, due to the fact that high-melting minerals in DQ ash were reduced as the addition of YN ash increased.

The simulated ash fusion process for blending DQ ash with different ratios of YN ash was carried out with FactSage software. Figure 5 displays the composition variations of the mixed ash under reducing atmosphere at 1100 °C. The percentage of $CaAl_2Si_2O_8$ kept growing with the content of YN ash increasing and reached its maximum at the addition of 40 wt % YN ash. Meantime, the proportions of SiO_2, FeV_2O_4, and V_2O_3 gradually decreased. $NaAlSiO_4$ appeared when the content of YN ash was more than 40 wt %. The content of V_2O_3 was only 4.2 wt %, and FeV_2O_4 was decomposed with 60 wt % YN ash addition. These simulated results were basically consistent with the XRD patterns of the mixture of DQ and YN ashes.

Phase assemblage for the above-mentioned mixed ashes calculated by FactSage software at different temperatures is shown in Figure 6. It can be seen from Figure 6a that only Ni and V_2O_3 in the blended ash were relatively stable with 10 wt % YN ash, whereas $CaAl_2Si_2O_8$, SiO_2, FeV_2O_4, and clinopyroxene were decomposed at high temperatures, which convinced that Ni and V_2O_3 as high-melting minerals affected AFTs of the mixed ash. Also, a similar situation exists in Figure 6b. Nepheline appeared in Figure 6c and melted at 1150 °C, meaning little impact on the AFTs of ash slag. In addition, SiO_2 was absent throughout the whole temperature range. Wollastonite and gehlenite were detected with their melting points both below 1150 °C in Figure 6d. Due to the high V content in DQ ash, V-rich spinel with high melting point was formed,[2,23,24] and completely disappeared at around 1300 °C in Figure 6e,f, which may explain why the AFTs for mixed ash slag decreased slowly when the addition of YN ash was over 50 wt %.

It can be concluded that Ni and V_2O_3 in the mixed ash slag remained stable even at high reducing temperatures, causing the high AFTs. Both possessed a trend of decreasing with the increasing YN ash addition. Thereafter, wollastonite, gehlenite, and V-rich spinel were found in the ash slag. The occurrence of V-rich spinel may have an effect on the AFTs of the blended ash to some extent.

3.4. Mineral Transformation Behaviors of DQ Ash Blending with SD Ash. The composition analysis for DQ ash mixed with different ratios of SD ash was carried out under the reducing atmosphere of 1100 °C, and the corresponding XRD patterns are displayed in Figure 7. With SD ash ranging from 10 to 40 wt %, the content of FeV_2O_4 increased and V_2O_3 decreased. V in DQ ash reacted with Fe in SD ash to form FeV_2O_4, causing that the content of high-melting V_2O_3 was decreased and the AFTs of the blended ash were further lowered, which also explained the phenomenon that the AFTs of the mixed ashes with 10 wt % SD ash increased slightly in Figure 1b. FeV_2O_4 reached its maximum under 40 wt % addition of SD ash. Besides, the increasing content of SD ash promoted the

https://doi.org/10.1021/acsomega.4c04453
ACS Omega 2024, 9, 33090−33098

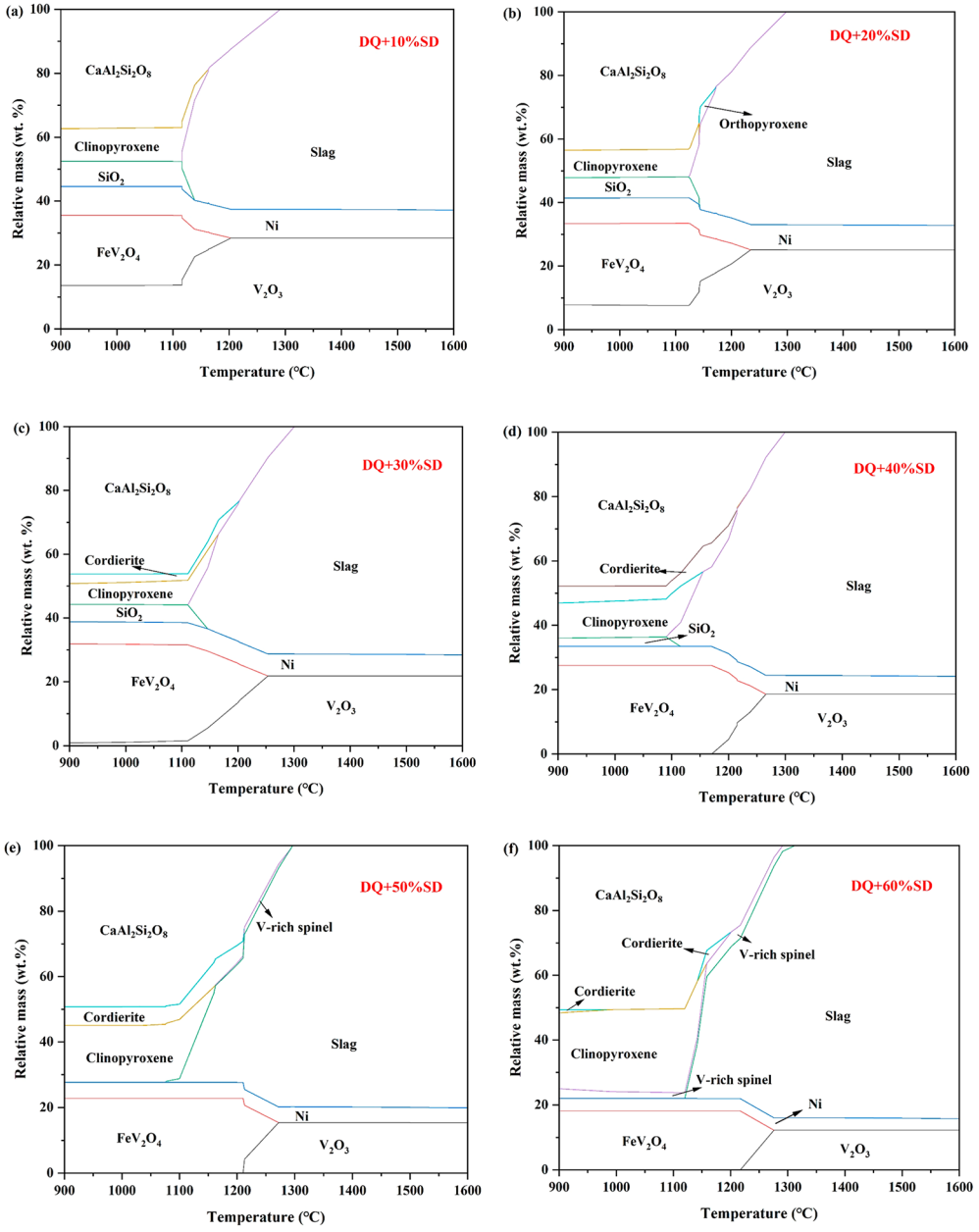

Figure 9. Phase assemblages of the mixed ashes with different ratios of SD ash at different temperatures simulated by FactSage: (a) DQ+10%SD, (b) DQ+20%SD, (c) DQ+30%SD, (d) DQ+40%SD, (e) DQ+50%SD, and (f) DQ+60%SD.

decrease of SiO_2 and the increase of $CaAl_2Si_2O_8$, which were beneficial to the decline of AFTs.

In Figure 8, the composition distributions for DQ ash blending with different ratios of SD ash were analyzed by FactSage software under reducing atmosphere at 1100 °C. When the addition of SD ash steadily increased, the variation tendencies of SiO_2, $CaAl_2Si_2O_8$, and FeV_2O_4 were similar to those of the XRD results in Figure 7. In addition, $3Al_2O_3{\cdot}2SiO_2$ showed a slight increase. Lowering the AFTs of the blended ash was caused by the continuous decrease in high-melting V_2O_3 and Ni.

Phase assemblage for mixing DQ ash with different contents of SD ash was calculated by FactSage software under the different temperatures, as shown in Figure 9. In Figure 9a, with the content of 10 wt % SD ash, the ash slag mainly consisted of clinopyroxene, $CaAl_2Si_2O_8$, SiO_2, FeV_2O_4, V_2O_3, and Ni under the set temperature ranges, which much resembled pure DQ ash. As the temperatures increased, some of the minerals melted and FeV_2O_4 completely decomposed at around 1200 °C. In contrast, the content of V_2O_3 kept growing. Although the temperature exceeded 1300 °C, Ni and V_2O_3 can exist steadily, leading to high ATFs of the ash slag. In Figure 9b, the formation of orthopyroxene was predicted. In Figure 9c, cordierite appeared, which then increased continuously and reached its maximum at 50 wt % addition of SD ash. There appeared V-rich spinel appears in Figure 9e, and it exhibited an increasing trend.

For all the simulated samples, the high-melting minerals were V_2O_3 and Ni in the ash slag above 1300 °C. With the temperature below 1100 °C and the content of SD ash between 10 and 30 wt %, V_2O_3 decreased slowly. Additionally, when the SD ash was over 50 wt %, V_2O_3 did not exist below 1200 °C but reappeared when the temperature was above 1200 °C. In general, the contents of V_2O_3 and Ni were decreased when the different ratios of SD ash were added as flux to DQ ash, resulting

https://doi.org/10.1021/acsomega.4c04453
ACS Omega 2024, 9, 33090−33098

in an overall decline of AFTs. When SD ash was gradually increased, SiO_2 showed a decreasing trend and finally vanished at 50 wt % addition of SD ash. Meanwhile, the content of FeV_2O_4 increased slowly and afterward reached its maximum when the content of SD ash ranged from 10 to 40 wt %. Thereafter, FeV_2O_4 decreased for samples with 50 and 60 wt % addition of SD ash.

4. CONCLUSIONS

In this work, the influence of high calcium coal and high iron coal on ash fusion characteristics of petroleum coke under a reducing atmosphere was investigated. The main conclusions are listed below:

(1) DQ ash has high AFT, and both YN and SD ash could effectively reduce the AFTs of DQ ash.

(2) DQ ash primarily consists of V_2O_3, SiO_2, $CaAl_2Si_2O_8$, FeV_2O_4, and Ni at 1100 °C under reducing atmosphere. As the temperature rises, the ash slag melts, and minerals (FeV_2O_4, V_2O_3, and Ni) with high melting points still exist, leading to high AFTs of DQ ash.

(3) With the addition of YN ash, the mixed ash has similar components to those of DQ ash. The content of SiO_2, FeV_2O_4, and V_2O_3 with high melting points gradually decreases due to the increasing content of YN ash, and thus the AFT of the mixed ash shows a decline.

(4) The mixed ash is mainly composed of V_2O_3, FeV_2O_4, SiO_2, Ni, and $CaAl_2Si_2O_8$ when DQ ash is blended with SD ash. With the content of SD ash increasing, Ni and V_2O_3 are steadily in decline, resulting in decreased AFT of the mixed ash. In particular, FeV_2O_4 keeps increasing and reaches its maximum under 40 wt % addition of SD ash.

AUTHOR INFORMATION

Corresponding Author

Bing Wang − *School of Electric Power, Civil Engineering and Architecture, Shanxi University, Taiyuan 030006, China;* orcid.org/0000-0003-0192-8436; Email: wangbing@sxu.edu.cn

Authors

Cuiyu Zhao − *Department of Architecture and Environmental Engineering, Taiyuan University, Taiyuan 030032, China*

Congxiu Guo − *School of Electric Power, Civil Engineering and Architecture, Shanxi University, Taiyuan 030006, China*

Complete contact information is available at: https://pubs.acs.org/10.1021/acsomega.4c04453

Notes

The authors declare no competing financial interest.

ACKNOWLEDGMENTS

The project was supported by Fundamental Research Program of Shanxi Province (No. 202303021222038), and Scientific and Technological Innovation Programs of Higher Education Institutions in Shanxi (No. 2021L006 and 2021L014).

REFERENCES

(1) Wang, B.; Li, W.; Ma, C.; Yang, W.; Pudasainee, D.; Gupta, R.; Sun, L. S. Synergistic effect on the co-gasification of petroleum coke and carbon-based feedstocks: A state-of-the-art review. *J. Energy Inst.* **2022**, *102*, 1−13.

(2) Wang, Z. G.; Kong, L. X.; Bai, J.; Li, H. Z.; He, C.; Yan, T. G.; Guo, Z. X.; Bai, Z. Q.; Li, W. Effect of vanadium and nickel on iron-rich ash fusion characteristics. *Fuel* **2019**, *246*, 491−499.

(3) Shen, F. H.; Qu, S. M.; Li, J. Y.; Yang, Z. H.; Zhou, C. G.; Yang, F.; He, Z. Q.; Xiang, K. S.; Shi, M. Q.; Liu, H. Development of chemical looping desulfurization method for high sulfur petroleum coke. *Fuel* **2024**, *357*, No. 129658.

(4) Wang, Z. G.; Bai, J.; Kong, L. X.; Bai, Z. Q.; Li, W. Effect of V and Ni on Ash Fusion Temperatures. *Energy Fuels* **2013**, *27* (12), 7303−7313.

(5) Sun, J. W.; Zhang, J. C.; Xu, D. L.; Zhang, S.; Lv, P.; Jiang, Y.; Song, X. D.; Kontchouo, F. M. B.; Jiao, Y.; Li, B.; et al. Synergistic effect mechanism of biomass ash-derived K-Ca-Si catalytic system on syngas production and reactivity characteristics of high-sulfur petroleum coke gasification. *Fuel* **2024**, *365*, No. 131224.

(6) Liu, M.; Li, F. H.; Liu, H. F.; Wang, C. Synergistic effect on co-gasification of chicken manure and petroleum coke: An investigation of sustainable waste management. *Chem. Eng. J.* **2021**, *417*, No. 128008.

(7) Nakano, J.; Duchesne, M.; Bennett, J.; Kwong, K.; Nakano, A.; Hughes, R. Thermodynamic effects of calcium and iron oxides on crystal phase formation in synthetic gasifier slags containing from 0 to 27 wt.% V_2O_3. *Fuel* **2015**, *161*, 364−375.

(8) Murthy, B. N.; Sawarkar, A. N.; Deshmukh, N. A.; Mathew, T.; Joshi, J. B. Petroleum Coke Gasification: A Review. *Can. J. Chem. Eng.* **2014**, *92* (3), 441−468.

(9) Li, W.; Wang, B.; Nie, J.; Yang, W.; Sun, L. S.; Pudasainee, D.; Gupta, R. Effect of the Composition of Additive Ash on the Thermal Behavior of Petroleum Coke Ash during Gasification. *Energy Fuels* **2020**, *34* (10), 12126−12134.

(10) Li, J. Z.; Xiong, Q. A.; Shan, J.; Zhao, J. T.; Fang, Y. T. Investigating a high vanadium petroleum coke ash fusibility and its modification. *Fuel* **2018**, *211*, 767−774.

(11) Frandsen, F.; Dam-Johansen, K.; Rasmussen, P. Trace elements from combustion and gasification of coal-An equilibrium approach. *Prog. Energy Combust. Sci.* **1994**, *20* (2), 115−138.

(12) Li, J. Z.; Zhao, J. T.; Zhang, L. X.; Liu, T.; Fang, Y. T. Transformation behavior of vanadium in petroleum coke during high temperature CO_2-gasification. *Fuel* **2017**, *194*, 83−90.

(13) Li, J. Z.; Zhao, J. T.; Dai, X.; Bai, J.; Fang, Y. T. Effect of Vanadium on the Petroleum Coke Ash Fusibility. *Energy Fuels* **2017**, *31* (3), 2530−2537.

(14) Ren, L. W.; Wei, R. D.; Zhu, T. C. Co-gasification reactivity of petroleum coke with coal and coal liquefaction residue. *J. Energy. Inst.* **2020**, *93* (1), 436−441.

(15) Song, H.; Yang, H. P.; Zhao, C.; Hu, J. H.; Zou, J.; Wu, P.; Li, S. Q.; Chen, H. P. Co-gasification of petroleum coke with coal at high temperature: Effects of blending ratio and the catalyst. *Fuel* **2022**, *307*, No. 121863.

(16) Wang, M.; Wan, Y. L.; Guo, Q. H.; Bai, Y. H.; Yu, G. S.; Liu, Y. R.; Zhang, H.; Zhang, S.; Wei, J. T. Brief review on petroleum coke and biomass/coal co-gasification: Syngas production, reactivity characteristics, and synergy behavior. *Fuel* **2021**, *304*, No. 121517.

(17) Li, J. L.; Wang, Y. F.; Zhu, L. C.; Zhang, Z. F.; Xiao, H. X. Experimental study on co-pyrolysis of petroleum coke and coals: Synergy effects and co-gasification reactivity. *Fuel* **2020**, *279*, No. 118368.

(18) Kang, J.; Zhao, L. H.; Li, W. W.; Song, Y. C. Artificial neural network model of co-gasification of petroleum coke with coal or biomass in bubbling fluidized bed. *Renewable Energy* **2022**, *194*, 359−365.

(19) Wang, R. K.; Zhao, Z. H.; Yin, Q. Q.; Wang, Z. Y. Influences of different fractions of extracellular polymeric substances on the co-slurrying properties of sewage sludge with coal and petroleum coke. *Energy Convers. Manage.* **2017**, *148*, 668−679.

(20) Kaneko, T. K.; Zhu, J. X.; Howell, N.; Rozelle, P.; Sridhar, S. The effects of gasification feedstock chemistries on the infiltration of slag into the porous high chromia refractory and their reaction products. *Fuel* **2014**, *115*, 248−263.

(21) Bunt, J. R.; Waanders, F. B. Trace element behaviour in the Sasol-Lurgi fixed-bed dry-bottom gasifier. Part 3-The non-volatile elements: Ba, Co, Cr, Mn, and V. *Fuel* **2010**, *89* (3), 537−548.
(22) Xiong, Q. A.; Li, J. Z.; Guo, S.; Li, G.; Zhao, J. T.; Fang, Y. T. Ash fusion characteristics during co-gasification of biomass and petroleum coke. *Bioresour. Technol.* **2018**, *257*, 1−6.
(23) Wang, Z. G.; Bai, J.; Kong, L. X.; Wen, X. D.; Li, X. M.; Bai, Z. Q.; Li, W.; Shi, Y. Viscosity of coal ash slag containing vanadium and nickel. *Fuel Process. Technol.* **2015**, *136*, 25−33.
(24) Duchesne, M. A.; Ilyushechkin, A. Y.; Hughes, R. W.; Lu, D. Y.; McCalden, D. J.; Macchi, A.; Anthony, E. J. Flow behaviour of slags from coal and petroleum coke blends. *Fuel* **2012**, *97*, 321−328.

https://doi.org/10.1021/acsomega.4c04453
ACS Omega 2024, 9, 33090−33098